Separation Shock Motion in Fin, Cylinder, and Compression Ramp—Induced Turbulent Interactions

D. S. Dolling* and L. Brusniak†
University of Texas at Austin, Austin, Texas

In conjunction with new experimental results at Mach 5, an examination has been made of published data on unsteadiness of shock-induced turbulent boundary-layer separation. The data are all wall pressure fluctuation measurements made under the unsteady separation shock and are from interactions induced by compression ramps, blunt and sharp fins, and circular cylinders. There is little evidence of a link between the separation shock zero-crossing frequency and characteristic frequency of the incoming boundary layer. The low shock frequencies and low shock speeds, and the trends with changes in model geometric parameters and incoming boundary layer, suggest that turbulent or global fluctuations at the upstream boundary of the separated flow drive the shock motion.

Nomenclature

d	= transducer diameter
d^+	= normalized transducer diameter ($\equiv du_\tau/\nu$)
D	= fin leading-edge diameter, cylinder diameter
f	= frequency
f_c	= shock zero-crossing frequency
$G(f)$	= power spectral density estimate
L_{sep}	= separated bubble length (ramp flows)
M_∞	= freestream Mach number
P_w	= instantaneous wall pressure
$\bar{P}_w$	= mean wall pressure
q_∞	= freestream dynamic pressure
Re_θ	= Reynolds number based on θ
$R_{pp}(\xi,\tau)$	= cross-correlation coefficient
t	= time
T_i	= time between consecutive shock passages
T_m	= mean time between consecutive shock passages
T_r, T_f, T_d	= time delays in "model" signal (Fig. 11)
u_τ	= friction velocity
U_c	= broadband convection velocity
U_∞	= freestream velocity
X	= streamwise distance from ramp corner or fin leading edge
α	= ramp corner angle, fin angle of attack
γ	= intermittency
δ	= boundary-layer velocity thickness
θ	= momentum deficit thickness
ν	= kinematic viscosity
ξ	= transducer spacing
σ_{Pw}	= standard deviation of wall pressure signal
τ	= time delay

Subscripts

o	= undisturbed conditions
max	= maximum value

I. Introduction

SINCE the early 1950's, it has been known that shock-induced turbulent boundary-layer separation is unsteady. In Bogdonoff's early work on step-induced interactions[1] and in the classic studies of Chapman et al.,[2] the unsteadiness was evident from randomly shot sequences of spark shadow and schlieren photographs and from high-speed cinema records. Such optical methods may readily reveal unsteadiness, but the results can be difficult to interpret because the photograph represents an integration of the light beam through a spanwise rippling shock structure. Consequently, little quantitative information has been obtained from them.

Most of what is known quantitatively comes from fluctuating wall pressure measurements. A typical wall pressure signal upstream of the separation location S (as indicated by surface tracers) in a nominally two-dimensional, Mach 3 unswept compression ramp flow is shown in Fig. 1a. The unsteady separation shock generates an intermittent pressure signal whose level fluctuates between that characteristic of the undisturbed turbulent boundary layer and that of the disturbed flow downstream of the shock wave. Kistler, in 1964, was probably the first to document this behavior.[4] The fraction of the time that a station in this intermittent region is downstream of the shock is given by the intermittency γ and increases in the downstream direction until just upstream of S, where $\gamma = 1.0$ (Fig. 1b). The moving shock generates a rapid increase in the wall pressure standard deviation σ_{Pw} upstream of S (Fig. 1c). The maximum occurs at $\gamma \approx 0.5$–0.7 and is a large fraction of the local $\bar{P}_w$.

Such pressure signals have been measured in flows generated by unswept compression ramps,[5-7] hemicylindrically blunted fins,[8] circular cylinders,[9] sharp fins at angle of at-

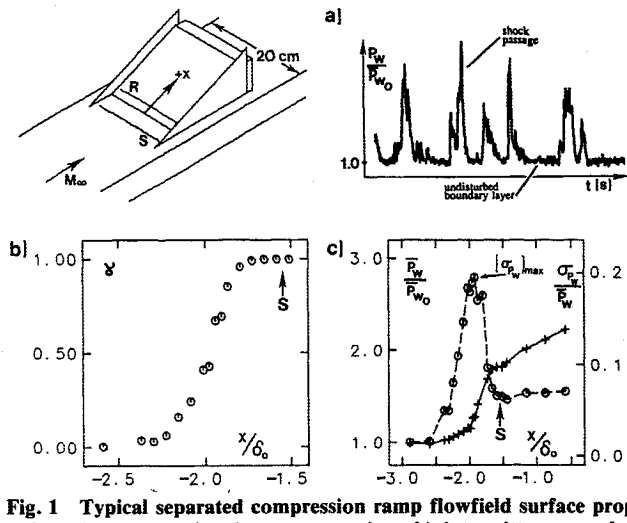

Fig. 1 Typical separated compression ramp flowfield surface properties: a) pressure signal near separation; b) intermittency; and c) mean wall pressure and standard deviation distributions.[3]

Received Aug. 31, 1987; revision received June 17, 1988.

*Associate Professor. Associate Fellow AIAA.
†Graduate Student. Student Member AIAA.

tack,[10-12] swept compression ramps,[12] and in shock-induced separation in transonic diffusers[13,14] and on transonic airfoils.[15] The distribution of σ_{Pw} has the same shape in all cases. Similar distributions have been reported in studies in which the pressure signal was not discussed explicitly, and thus its intermittent character can only be inferred. These include circular cylinders at transonic speeds,[16] impinging shock waves,[17] and axisymmetric flares and steps.[18,19] Hence, this phenomenon would appear to be an inherent feature of shock-induced turbulent separation.

One of the most fundamental questions about this unsteadiness is the driving mechanism. In the supersonic regime, this question has been addressed by several authors.[5,7,9,12] The results are confusing. For the Mach 3, 24-deg, compression ramp flow of Fig. 1, Andreopoulos and Muck concluded that "the incoming boundary layer is the most likely cause triggering the shock wave oscillation." This conclusion stemmed largely from two observations. First, results from a conditional sampling algorithm suggested that the shock zero-crossing frequency f_c (defined as the number of crossings per second of the transducer by the shock) was of the same order as the estimated bursting frequency in the incoming boundary layer. Second, the measured shock velocities were of the same order as velocity fluctuations in the flowfield. However, measurements made by Tran at the same freestream conditions in the same facility, but using a 20-deg ramp model, appear to suggest otherwise.[12] The 20-deg model generates a similar flowfield to the 24-deg case but has a smaller separated bubble. In Tran's experiment, one transducer was placed on the upstream influence line and the other upstream in the incoming turbulent boundary layer. The upstream channel was used as a trigger for sampling on the other, and the Variable Interval Time-Averaging (VITA) technique was used to analyze the data. There was little correlation between events detected on the upstream channel and the low frequency, large-amplitude pressure pulses on the downstream channel. Tran concluded that the pressure pulses in the intermittent region were independent of the large-scale structures in the upstream boundary layer. Similar results were obtained by Tran for a sharp-fin model at 20-deg angle of attack.[12]

Measurements in interactions generated by blunt fins at zero angle of attack, made in the same Mach 3 facility and with the same incoming boundary layer as the ramp tests, support Tran's findings.[9] In this case, f_c was found to be largely dependent on the fin leading-edge diameter D.[9] The streamwise length scale of the shock motion was found to be of $\mathcal{O}[D]$ and could vary from a fraction of δ_o to several δ_o, depending on the flowfield under study. Although these tests did not focus specifically on the driving mechanism, the results suggest a connection with the downstream flowfield (which is strongly influenced by D) rather than the incoming boundary layer (whose properties are fixed and independent of D).

In this paper, these and other published data have been reexamined in conjunction with some new results obtained by the current authors in interactions generated by circular cylinders at Mach 5. This reevaluation had two main objectives. The first was to attempt to clarify these conflicting results and determine what conclusions, if any, could be drawn about the cause of the shock motion. To do this, the various conditional sampling algorithms used for estimating f_c have been assessed to determine which are reliable. Power spectra of the incoming turbulent boundary-layer pressure fluctuations and those in the region of shock oscillation also have been examined to see if any obvious correspondences could be established. The few results from space-time correlations and other statistical techniques have also been examined. If no obvious driving mechanism was identified, the second objective was to see if these results might provide some insight into the design of more highly focused, future experiments.

II. Experimental Data

The earlier experiments that have been examined will be referred to as flows 1 through 6 as listed in Table 1. The new Mach 5 experiment is flow 7. Complete experimental details are given in the cited references. Under the "Comments" column, *SC* indicates that only a single channel of pressure data was recorded; *MCn* indicates multichannel, where n is the number of simultaneously sampled channels. In all cases, Kulite pressure transducers were used. *FP* and *TF* under the column headed "δ_o" are explained below.

In brief, the Mach 3 experiments were conducted at a stagnation pressure of 6.8×10^5 Nm^{-2} (100 psia) ± 1% and stagnation temperature of 265 K ± 5% in the Princeton University 20 × 20-cm blowdown tunnel. Three test surfaces were used. These were 1) the tunnel floor in section 1 of the facility (indicated by *TF*1 in Table 1); 2) the tunnel floor in section 2, which is about 1 m further downstream (*TF*2); and 3) a full-span flat plate (*FP*). The new Mach 5 experiment was conducted on a full-span flat plat in the 17.8 × 15.2-cm blowdown tunnel of the University of Texas at Austin at a stagnation pressure and temperature of 2.1×10^6 Nm^{-2} ± 1% and 327 K ± 1%, respectively. In both facilities, the wall temperature was within 5% of the adiabatic value, and boundary-layer transition occurred naturally. The incoming velocity profiles developed in essentially zero pressure gradient and fitted the combined law-of-the-wall-law-of-the-wake well with skin fric-

Table 1 Experimental data set

Flow	M_∞	δ_o, cm	Re_θ	Geometry	Comments	Refs.
1	3	0.44 (*FP*) 1.6 (*TF*1)	14,800 56,000	Blunt fin, D = 1.27, 2.54 cm	Data on centerline, (*SC*)	8,9
2	3	1.2 (*TF*1) 2.2 (*TF*2)	41,600 71,500	Unswept compression ramp, Ramp angle α = 24 deg	Separated flow, ($L_{sep} \approx 2.2\delta_o$) (*SC*)	5
3	3	2.2 (*TF*1)	71,500	Unswept compression ramp, α = 16, 20, 24 deg	16 deg, incipient separation 20 deg, $L_{sep} \approx 0.7\delta_o$ 24 deg, $L_{sep} \approx 2.2\delta_o$(*SC*)	3
4	3	2.4 (*TF*2)	84,500	Unswept compression ramp, α = 24 deg	Separated flow, ($L_{sep} \approx 2.2\delta_o$) (*MC*4)	6
5	3	2.4 (*TF*2)	84,500	Unswept compression ramp, α = 24 deg	Separated flow, ($L_{sep} \approx 2.2\delta_o$) (*MC*4)	7
6	3	1.7 (*TF*2)	59,000	Sharp fin, angle of atack, α = 12, 16, 20 deg	Measurements made at spanwise stations $1.9\delta_o$ and $5.1\delta_o$ from leading edge (*MC*4)	10,12
7	5	0.54 (*FP*)	9,000	Unswept circular cylinder, D = 1.27, 1.91 cm	Data on centerline, *MC*2	9

tion coefficients within ± 10% of those from Van Driest II theory. In all cases, the wake-strength parameter $\bar{A}$ was within the accepted range of 0.4–0.6.

III. Discussion of Results

Incoming Turbulent Boundary Layer

In all of these studies, some information on the fluctuations in the incoming boundary layer is provided. In the single-channel experiments, only σ_{Pw}, power spectral density estimates $G(f)$, and probability density distributions of the fluctuation amplitudes are given. In the multichannel experiments, space-time correlations were calculated, and estimates of the broadband convection velocity U_c are given. The values correlate well with incompressible and subsonic data (Fig. 10, Ref. 9). No unusual features are evident in any of the results. For further details, the reader is referred to Refs. 6 and 12.

At such high speeds, frequencies up to several hundred kHz are to be expected. Such high frequencies cannot be resolved for several reasons. First, the transducer size is finite. From measurements and correlations in incompressible and subsonic flows, Shewe[20] has shown that σ_{Pw}/q_∞ is a function of the normalized transducer diameter $d^+(d^+ \equiv du_\tau/\nu)$. The "ideal" transducer has $d^+ \approx 20$. For the Mach 3 and 5 studies, d^+ was about 300 and 200, respectively, even though the smallest available transducers were used. If Shewe's results apply in compressible flows, then σ_{Pw} is probably underestimated by about 50%. Second, the transducer bandwidth is limited by the natural frequency of its diaphragm and also by the protective screen above the diaphragm that shields it from dust particles.

At Mach 3, Muck et al.[6] estimated that spectra and correlations were valid up to 45–50 kHz ($\approx 2U_\infty/\delta_o$). In the new work at Mach 5, the bandwidth was similar but is only about 0.5 U_∞/δ_o. Since all of these studies focused on the shock motion, which occurs at a few kHz or less, the authors of these references rightfully claim that these limitations are not severe. However, it is clear that the undisturbed boundary-layer spectra are only well resolved at low frequencies, and values of σ_{Pw} are almost certainly seriously underestimated.

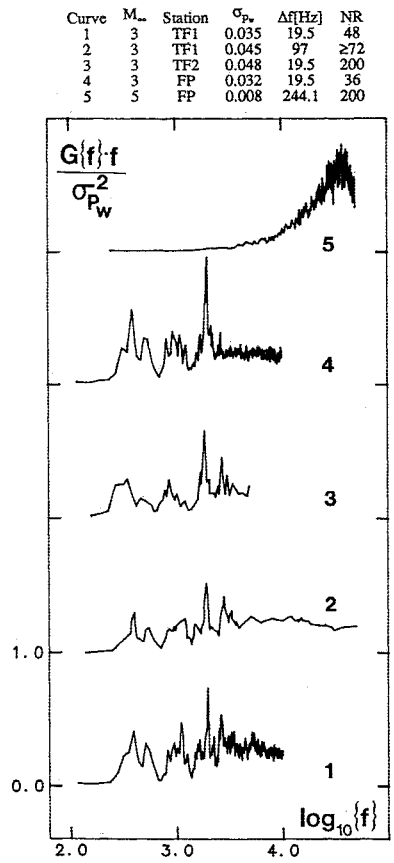

Fig. 2 Power spectra of incoming undisturbed turbulent boundary layers.

Power spectra are shown in Fig. 2. Curve 1 is plotted on the axes shown. All other curves are staggered 1 unit of $fG(f)/\sigma^2_{Pw}$ upwards. Curve 2 is from Ref. 12 where it was plotted in these coordinates; hence, it has simply been replotted. Curves 1, 4, and 5 were calculated by the current authors using the original digital data. Curve 3 is from Fig. 8 of Ref. 6 where it was plotted as $G(f)$ vs f on log-log axes and has been rescaled. Where known, σ_{Pw}, the frequency resolution Δf, and the number of data records N_R used to calculate each spectrum are shown in the legend.

For consistency, all spectra in this paper are plotted on linear-log axes rather than as $G(f)$ vs f on log-log axes. The area under a given curve segment then is linearly proportional to the contribution of the respective frequency range to σ^2_{Pw} [i.e., $G\,df = (fG)\,df/f = (fG)\,d(\ln f) \neq \ln G\,d(\ln f)$], and dominant frequency ranges are more easily recognized. Because of the broadband nature of the boundary-layer pressure signal, this approach is not as useful as in the region of shock oscillation where most of the energy is in a narrow band. Normalizing by σ^2_{Pw} forces the area under the curve to unity and is useful for comparative purposes. Again, it is more useful in the region of shock oscillation where the true spectrum and true σ_{Pw} are more easily measured. If σ_{Pw} is underestimated, as in the undisturbed boundary layer, normalization may distort the spectrum and is, in general, less desirable. In this case, where the objective was to identify the frequency distributions of the fluctuation energy and any noise, rather than accurate absolute power levels, normalization should not be misleading.

Curves 1 and 2 were measured on the tunnel floor in section 1 at stations a few centimeters apart and illustrate the repeatability of flow conditions. Curve 1 was obtained in 1981 whereas curve 2 was measured using different transducers in 1987. Curve 3 is also on the tunnel floor but in section 2. The spectrum on the flat plate is given by curve 4. All four spectra are contaminated by noise in two bands centered around 0.3–0.5 and 0.9–1.2 kHz. In Ref. 12, Tran attributed this contamination to noise from the settling chamber, although no evidence to support this was provided. In addition, the four spectra have maxima in narrow bands centered around 1.9 and 2.7 kHz. The authors of Refs. 6 and 12 do not identify the cause of these either. In contrast, the Mach 5 spectrum (curve 5) has little, if any, low-frequency contamination. However, it is evident that the transducer only captures the low-frequency end of the spectrum.

Intermittent Region

Power spectra in the intermittent region have been reported for all of the flows in Table 1. Figure 3 shows the Mach 3 results at the location of $(\sigma_{Pw})_{max}$. Curves 1–3 are plotted on the scales shown, whereas curves 4–9 are successively shifted 0.3 units of $fG(f)/\sigma^2_{Pw}$ upwards. Curve 10 is a special case in which the power axis is $fG(f)$ in arbitrary units. However, the distribution of relative power is correct, so direct comparisons of the frequency content can be made with the other cases. The arrows labeled STM and TTM are explained in the next section. Curve 1 was given in Ref. 6 as $G(f)$ vs f whereas curves 4 and 5 were presented in the form $G(f)U_\infty/q^2_\infty\delta_o$ vs $f\delta_o/U_\infty$ in Ref. 3. In these three cases, data points were read from each plot, rescaled, and replotted. Curves 2, 3, 6, and 7 were calculated by the current authors from the original digital data whereas curves 8 and 9 were already in the form $fG(f)/\sigma^2_{Pw}$ in Ref. 12 and have simply been replotted. Where known, σ_{Pw}, Δf, and N_R are given in the legend.

The axes of Fig. 3 are the same as in Fig. 2 and were chosen for the reasons outlined earlier. It is probably confusion over appropriate axes that is responsible for the observation in Refs. 6 and 7 that, for the 24-deg compression ramp flow

Curve	Stat./Geom.	σ_{P_w}	Δf[Hz]	NR
1	2/24° ramp	0.85	39	-
2	2/24° ramp	0.80	488	750
3	1/24° ramp	0.72	488	600
4	2/20° ramp	0.64	195	200
5	2/16° ramp	0.47	195	200
6	1/D=1.27 cm	0.70	156	36
7	1/D=2.54 cm	0.84	156	36
8	1/16° sharp fin	0.21	97	≥72
9	1/20° sharp fin	0.33	97	≥72
10	1/12° sharp fin	-	97	≥72

- indicates unknown; σ_{p_w} in psi

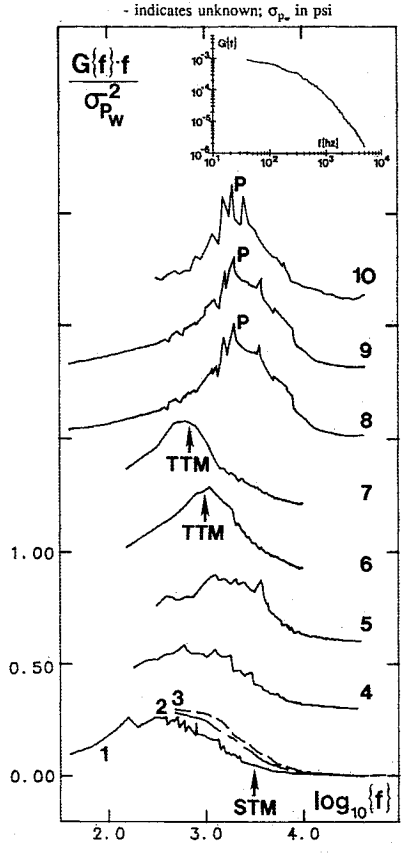

Fig. 3 Power spectra at $(\sigma_{Pw})_{max}$ in intermittent region (Mach 3, tunnel floor).

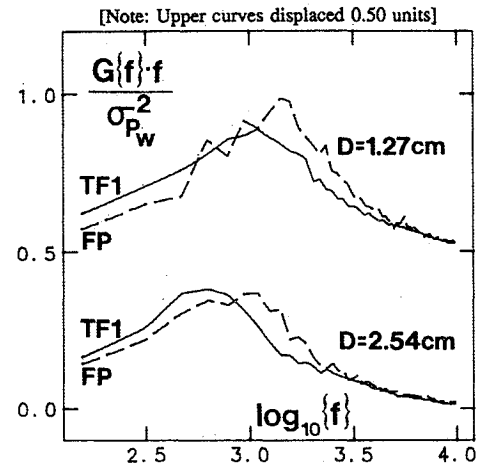

Fig. 4 Power spectra at $(\sigma_{Pw})_{max}$ in intermittent region (Mach 3, tunnel floor and flat plate).

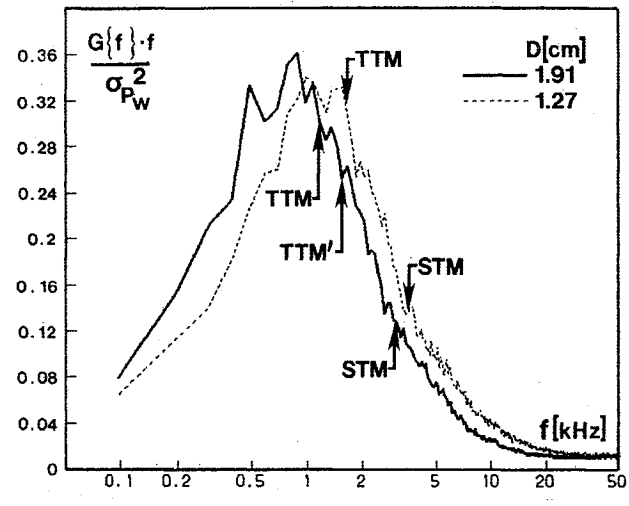

Fig. 5 Power spectra at $(\sigma_{Pw})_{max}$ in intermittent region (Mach 5, flat plate).

(curve 1), the "spectra are broadband and show no evidence of a frequency peak." That such a conclusion could be easily drawn is illustrated in the inset of Fig. 3, which shows curve 1 in its original form, $G(f)$ vs f, plotted on log-log axes.

In all cases, the large amplitude shock-induced fluctuations are centered at relatively low frequencies. Consider first the 24-deg compression ramp results (curves 1-3). Curves 1 and 2 are in section 2 of the facility ($\delta_o = 2.2$ cm) and were measured in 1986 (Ref. 6) and 1983 (Ref. 3), respectively. In the earlier study, Δf was very large (488 Hz). Hence, curve 2 does not have a peak because the first spectral point is at the approximate peak location. In the later study, Δf was as low as 10 Hz, resulting in a well-defined maximum. Despite the poor resolution of curve 2, agreement with curve 1 at the higher frequencies is good (their displacement is due to differences in σ^2_{Pw}). These differences probably occur because the gradient is steep near $(\sigma_{Pw})_{max}$, and small differences in transducer position lead to large differences in σ^2_{Pw}. Curve 3 was measured about 1 m further upstream ($\delta_o = 1.2$ cm) and does not have a peak for the same reasons. Within experimental accuracy, curves 2 and 3 are essentially the same. Whether their maxima coincide cannot be stated with certainty, but it seems unlikely that the two curves would differ significantly in the narrow band below 488 Hz.

Curve 1 shows that the shock frequency is centered around 0.3-0.4 kHz. Since the incoming boundary layer has significant energy noise in this same low-frequency range (curve 1, Fig. 2), this might, by itself, suggest a link with the shock motion. However, in the same boundary layer a decrease in ramp angle to 20 deg (curve 4), which reduces the length of the separated bubble from $2.2\delta_o$ to $0.7\delta_o$, increases the center frequency to the range of 0.5-1.8 kHz. A further decrease in ramp angle to 16 deg, which corresponds to incipient separation, also increases the center frequency (curve 5). It is less well defined for this case but is in the range of 1-3 kHz. Since the incoming boundary-layer properties are fixed but the spectrum center frequency varies, these data do not support the idea of a simple correlation with the bursting frequency. More will be said about this later.

Curves 6 and 7 are for blunted fins ($D = 1.27$ and 2.54 cm, respectively) in the tunnel-floor boundary layer (section 1, $\delta_o = 1.6$ cm). In blunt-fin flows, most of the important time-averaged interaction length scales in the streamwise, spanwise, and vertical directions depend primarily on D.[21] Doubling D doubles the centerline upstream influence, the separation length, and the primary vortex scale. It can be seen that the power spectrum in the intermittent region also is affected by D. The normalized maximum power level remains the same, but the center frequency decreases from about 1.1 to 0.6 kHz as D increases. The same fins were also tested on a flat plate under identical freestream conditions as the tunnel-floor tests. The spectra at $(\sigma_{Pw})_{max}$ on both test surfaces are shown in Fig. 4. In the thinner boundary layer on the plate, the center frequency increases; from 0.6 kHz to about 1 kHz for $D = 2.54$ cm and from 1.1 to 1.4 kHz for $D = 1.27$ cm. If low-frequency noise was the trigger, then similar center frequencies might be anticipated, since the noise is at the same frequencies in both boundary layers. The increase in center

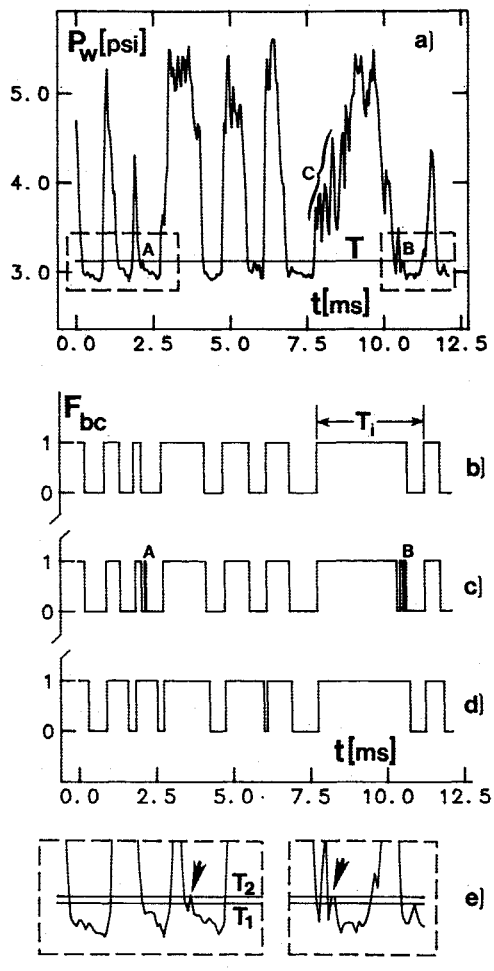

Fig. 6 Conversion of pressure signal into boxcar function: a) original signal; b) boxcar judged by eye; c) boxcar from STM; d) boxcar from TTM; and e) problem associated with closely spaced thresholds.

frequency for fixed D suggests that it is not. Additional evidence to support this comes from the new Mach 5 cylinder tests. Spectra at $(\sigma_{Pw})_{max}$ are shown in Fig. 5. There is little, if any, low-frequency noise in the incoming boundary layer (curve 5, Fig. 2), yet the center frequencies are in the same range as at Mach 3 (0.8–1.3 kHz for the 1.27-cm case and 0.5–1 kHz for the 1.91-cm diam model). The decrease in center frequency with increasing D is consistent with the Mach 3 results.

Spectra at $(\sigma_{Pw})_{max}$ for the sharp-fin flows at $\alpha = 16$ and 20 deg are given by curves 8 and 9 (Fig. 3), respectively. Curve 10, for $\alpha = 12$ deg, as noted earlier, has the correct distribution of relative power but has the power in arbitrary units. The three spectra are almost identical with a common center frequency of about 2 kHz. (The sharp peak, labeled P, at a frequency of 2.7 kHz and common to all 3 cases is also evident in the undisturbed boundary layer and therefore is not generated by the shock motion.) Possible reasons for these higher values and their independence of angle of attack are suggested later.

These data have two interesting features. First, typical large eddy frequencies in these incoming boundary layers vary from about 30–40 kHz yet the shock center frequencies are very low, ranging from a few hundred Hz to about 2 kHz. Second, with a fixed boundary layer the center frequency depends on the particular interaction studied, be it generated by a ramp or a blunt or sharp fin. Neither of these observations supports a direct correlation of the shock center frequency with the boundary-layer bursting frequency.

Conditional Sampling Algorithms

To isolate the shock-motion component of the pressure signal, several authors have employed conditional sampling

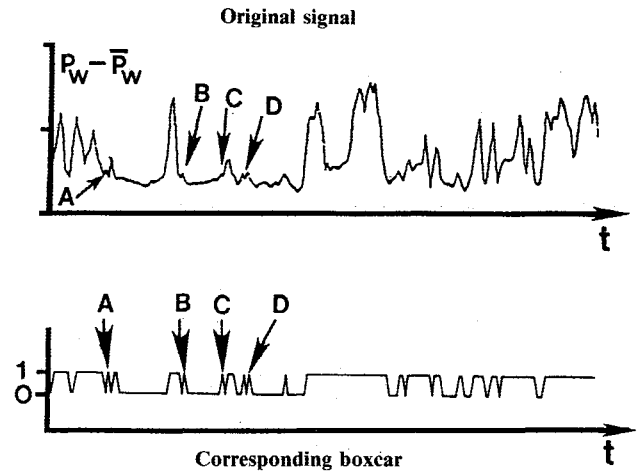

Fig. 7 Application of STM algorithm to Mach 3, 24-deg compression ramp pressure signal.

algorithms.[5,7,9,12] Their common feature is the conversion of the pressure signal (Fig. 6a) into a "boxcar" of amplitude unity and varying frequency (Fig. 6b). The time T_i between consecutive passages of the shock over the transducer then can be determined and statistics performed to obtain the probability distribution of T_i and the mean value

$$T_m \left(\equiv \frac{1}{N} \sum_{i=1}^{N} T_i \right)$$

where N is the number of periods. It should be noted that $1/T_m$ is the shock zero-crossing frequency f_c, not the mean shock frequency f_m, which is given by

$$\frac{1}{N} \sum_{i=1}^{N} f_i$$

where $f_i = 1/T_i$. Since the pressure signal is of a turbulent flow, precautions must be taken to ensure that high-frequency turbulent fluctuations are not inadvertently counted as shock waves. This problem, and others, and some results from these techniques are discussed below.

Single-Threshold Methods (STM)

In earlier work by the first author,[5] a single threshold T was used, as indicated in Fig. 6a. T was set equal to $\bar{P}_{wo} + 3\sigma_{Pwo}$, where subscript o refers to the undisturbed boundary layer. Thus, when P_w increased above the maximum pressure of the undisturbed boundary layer, this indicated the start of the shock passage upstream over the transducer. When P_w fell below T, this indicated the end of the shock passage. However, because drift and zero shifts cause small dc offsets from test to test, the results can be inaccurate. Andreopoulos and Muck[7] improved on this by "eyeballing" each signal and choosing T just above the largest fluctuations of the boundary-layer component of the signal. This was the technique used by them in flow 5, and T_m was found to be approximately $7.7\delta_o/U_\infty$ and independent of position in the intermittent region and ramp angle (i.e., independent of downstream flow conditions), and f_c was equal to $0.13U_\infty/\delta_o$, which the authors claim is of the same order as the estimated bursting frequency of the turbulent boundary layer. As mentioned in Sec. I, this apparent correlation with the bursting frequency was one of the reasons that led these authors to conclude that "the incoming boundary layer is the most likely cause triggering the shock wave oscillation."

Although this method does avoid the difficulties noted above, a far more serious problem with using a single threshold is that many "false shocks" are counted. Figure 6 illustrates the problem. Figure 6b shows the "ideal" boxcar, as judged by eye, for the pressure signal in Fig. 6a. Figure 6c

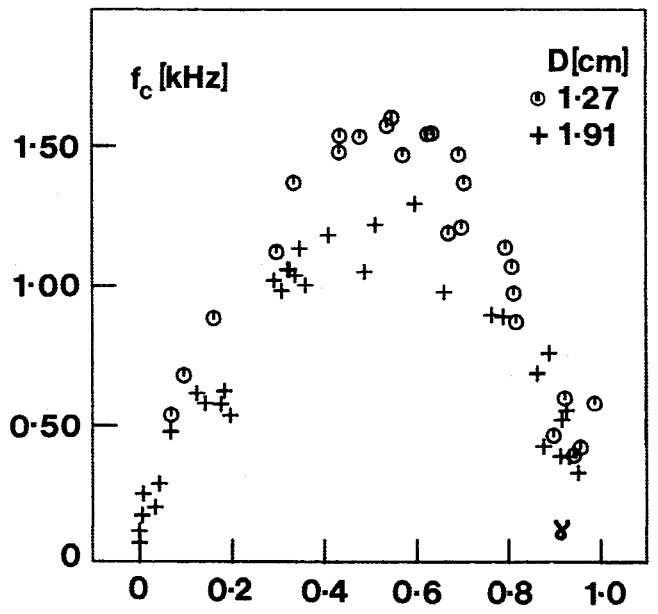

Fig. 8 Shock zero-crossing frequency as a function of intermittency (cylinders, Mach 5).

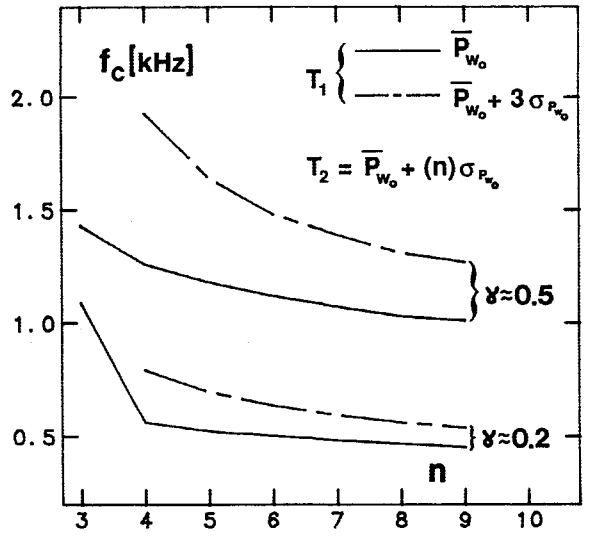

Fig. 9 Sensitivity of f_c to threshold settings for TTM.

shows the STM boxcar, in which turbulent fluctuations such as A and B (Fig. 6a) are inadvertently counted as shock waves. A second example (Fig. 7), resketched from data presented by Andreopoulos and Muck to illustrate their method, shows the inclusion of four "shock waves," labeled A, B, C, and D, which are not in the original signal. Because these "shocks" are actually turbulent fluctuations, they occur at high frequency and drive f_c higher. In practice, no matter what level T is set at, fluctuations such as A and B or the series around C (Fig. 6a) will always result in this problem. That it is significant can be seen by locating the value of f_c ($0.13U_\infty/\delta_o \approx 3.1$ kHz) on the corresponding power spectrum in Fig. 3. This value, indicated by the arrow labeled STM, is actually around the upper boundary of the shock frequency range.

This result, and the earlier observation that the spectrum center frequency in this case is about 0.3–0.4 kHz, casts doubt on the correlation of the shock frequency with the bursting frequency and the proposed linkage of the shock motion with "bursting" in the incoming boundary layer.

Two-Threshold Methods (TTM)

To avoid the problems above, an algorithm using two thresholds was used to analyze the new Mach 5 experiments and reexamine earlier results for which the original digital data were available. In this case, the upper threshold $T_2 = \bar{P}_{wo} + 4.5\sigma_{Pwo}$ and the lower one $T_1 = \bar{P}_{wo}$.

To determine $\bar{P}_{wo}$, a "window" of width ΔP was stepped upwards through the pressure signal in small increments, starting at the minimum value. At each step, the number of data points within the window is counted. Since the measured fluctuations in the undisturbed boundary-layer component of the signal are distributed essentially normally, the position at which the greatest number of data points occurs brackets $\bar{P}_{wo}$. The standard deviation σ_{Pwo} of the boundary-layer component of the signal then is calculated. Since the probability of finding points $4.5\sigma_{Pwo}$ above $\bar{P}_{wo}$ is very low (i.e., 0.0000068) according to a Gaussian distribution, $\bar{P}_{wo} + 4.5\sigma_{Pwo}$ was chosen for T_2. Hence, $P_w > T_2$ is characteristic of the flow downstream of the shock, and $P_w < T_2$ is characteristic of the undisturbed boundary layer. This approach requires no subjective input from the user and sets T_2 consistently just above the largest fluctuations of the boundary layer. It automatically takes care of dc offsets or drift from run to run.

Initially, if $P_w < T_2$, a flag is set "off." The algorithm then checks successive data points. If the first point is less than T_2 and the second point is greater than T_2 and the flag is "off," this marks the start of the shock passage. The counter that records the time between successive shock waves is initialized, and the flag is set "on." Further crossings of T_2 are not counted until $P_w < T_1$. Termination of the shock wave occurs when this happens, and the flag is reset. As shown in Fig. 6d, this process largely eliminates the counting of turbulent fluctuations as shock waves. Under some circumstances, it is probable that the same result could be obtained by digital filtering. However, since in this case the higher shock frequencies f_i and lower frequencies of the turbulent pressure fluctuations overlap, use of digital filtering would eliminate the higher-frequency shocks.

Distributions of f_c using the TTM for the Mach 5 cylinder flows are shown in Fig. 8. Unlike the Mach 3 compression ramp results in Ref. 7, which may reflect the inadequacies of the STM, f_c is strongly dependent on position in the intermittent region and is a maximum at $\gamma \approx 0.5$ in both cases; about 1.6 kHz for $D = 1.27$ cm and about 1.2 kHz for $D = 1.91$ cm. These values are indicated by arrows labeled TTM on the power spectra in Fig. 5 and fall close to the center frequency. Values of f_c also were calculated using the STM and are indicated by arrows labeled STM in Fig. 5. They are significantly higher than the center frequency. This again suggests that the calculated values of f_c in Ref. 7 are unreliable. The same TTM algorithm also was used by the current authors to reexamine the data taken in the Mach 3 blunt-fin flows (flow 1). With only a few measurement stations in the intermittent zone, neither the distribution of f_c nor $(f_c)_{max}$ could be defined very accurately. For $D = 1.27$ and 2.54 cm, $(f_c)_{max}$ was estimated to be about 1 and 0.7 kHz, respectively. These values are indicated by TTM on the spectra (Fig. 3) and are consistent with the Mach 5 results. However, whereas the spectra (Fig. 4) show a shift towards higher frequencies for the thinner boundary-layer case, this was not evident in the plots of f_c vs γ and is probably attributable to resolution problems. Since the original digital data were unavailable, the TTM could not be used for any of the other flows.

Although this approach largely avoids counting turbulent fluctuations as shock waves, it can be seen that if two shock passages occur close together then P_w may not fall below $\bar{P}_{wo}$ before increasing again, the flag will not be reset, and two shock passages will be counted as one. To examine this, and also assess the sensitivity of f_c to T_1 and T_2, the latter were systematically varied. First, with $T_1 = \bar{P}_{wo}$, T_2 was set equal to $\bar{P}_{wo} + n\sigma_{Pwo}$, $3 \le n \le 9$. Next, T_1 was increased to $\bar{P}_{wo} + 3\sigma_{Pwo}$ and T_2 varied as before. With this higher value of T_1, the shock counter is reset when P_w falls within the range of the turbulent boundary-layer fluctuations rather than below the mean value.

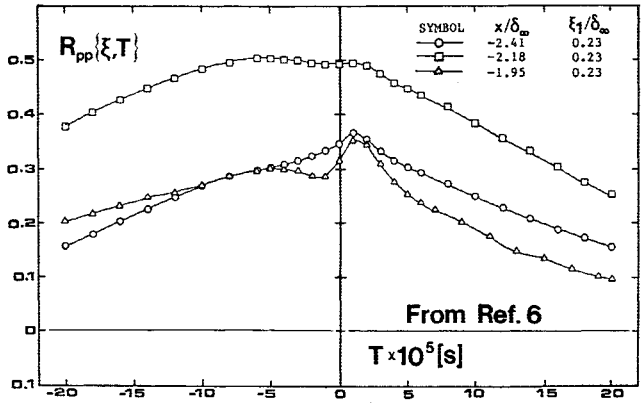

Fig. 10 Space-time correlations in 24-deg compression ramp flow (Mach 3).

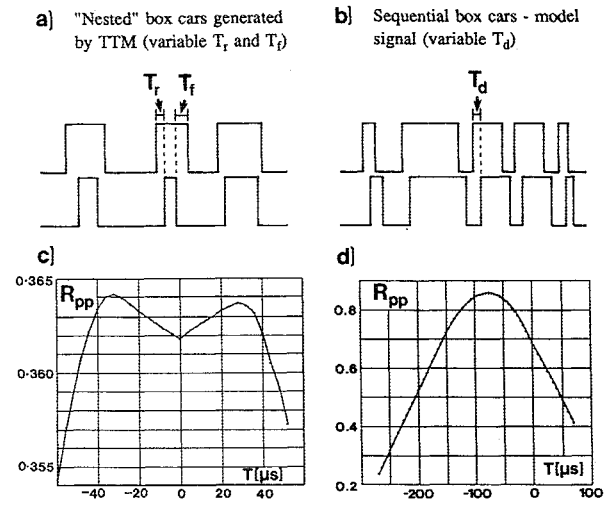

Fig. 11 Space-time correlations of nested and sequential "model" signals.

Results at $\gamma \approx 0.2$ and 0.5 for the Mach 5 cylinder flows are shown in Fig. 9. With $T_1 = \bar{P}_{wo}$, f_c is relatively insensitive to T_2 once T_2 is above the range of the boundary layer (i.e., $n > 3$). For a fixed T_2, f_c increases as T_1 is increased from $\bar{P}_{wo}$ to $\bar{P}_{wo} + 3\sigma_{Pwo}$, since P_w does not have to decrease as far to reset the counter. At low γ, when relatively long periods of undisturbed boundary-layer flow occur between successive shock passages, the choice of T_1 is less critical than at higher γ. At higher γ, when $T_1 = \bar{P}_{wo} + 3\sigma_{Pwo}$, T_2 must be set significantly higher than T_1 to avoid turbulent fluctuations (such as those in Fig. 6e) being counted as shock waves (i.e., if T_1 and T_2 are too close, the method becomes similar to the STM and has similar problems). If $T_2 = \bar{P}_{wo} + 6\sigma_{Pwo}$ or higher, f_c then is relatively insensitive to further increases in T_2.

It is evident that f_c cannot be pinpointed precisely but can be bracketed within a narrow range. The lower boundary of the range corresponds to the settings $T_1 = \bar{P}_{wo}$, $T_2 = \bar{P}_{wo} + 4.5\sigma_{Pwo}$, since this requires that P_w fall below $\bar{P}_{wo}$ between shock waves. The upper boundary is set by $T_1 = \bar{P}_{wo} + 3\sigma_{Pwo}$, $T_2 = \bar{P}_{wo} + 6\sigma_{Pwo}$. With these as bounds, f_c is 0.55–0.65 kHz at $\gamma \approx 0.2$, and 1.2–1.5 kHz at the higher γ. These upper bounds are indicated by TTM′ on the spectra of Fig 5.

In summary, the STM gives unrealistically high estimates of f_c due to its inability to distinguish turbulent fluctuations from shock waves. The TTM largely avoids this problem and with physically sensible choices of threshold settings, f_c can be bracketed within a fairly narrow range. Power spectra and the TTM algorithm both show that the shock zero-crossing frequencies are very low compared to characteristic frequencies in the incoming boundary layer. Large eddy time scales that are of order δ_o/U_∞ range from about 7-40 μs (26–140 kHz), yet the shock zero-crossing frequencies are typically 2 kHz or less. Further, with fixed incoming flow conditions, the shock frequencies depend on the model geometry suggesting a link with the downstream separated flowfield rather than the incoming boundary layer.

Space-Time Correlations/Shock Velocities

Longitudinal space-time correlations $R_{pp}(\xi,\tau)$ calculated by Muck et al.[6] in the Mach 3, 24-deg compression ramp flow are shown in Fig. 10. The spacing ξ between transducers is 0.23 δ_o. The case $X/\delta_o = -2.18$ has the upstream transducer at $(\sigma_{Pw})_{max}$ and highlights the features of such correlations and the difficulties of interpretation. One source of difficulty is that two different physical phenomena occur together. There is shock motion in the upstream and downstream directions superposed on convective transport of turbulent eddies largely in the downstream direction. This leads to difficulties in interpreting the values of τ at which maxima in R_{pp} occur.

The correlation at $X/\delta_o = -2.18$ has two maxima; one at $\tau \approx -60$ μs and one at $\tau \approx +10$ μs. The other two curves also exhibit the latter, which is due to turbulent eddy convection downstream. This is evident from correlations in the incoming boundary layer (Fig. 3, Ref. 6), since the maximum in R_{pp} is at essentially the same positive τ. Muck et al.[6] suggested that the maximum at negative τ is "probably due to the shock motion." Results from the new study at Mach 5 confirm this. In this case, correlations were performed on the original signals, the boxcars generated by the TTM (in which all turbulence information is eliminated), and a set of model signals. The model signals were either "nested" square waves (as are generated by the TTM) with variable rise and fall times T_r and T_f (Fig. 11a) or "sequential" square waves with the delay time T_d fixed for a given pair of waves but varying through the signal (Fig. 11b). These two signal types have different cross correlations with different physical interpretations. For nested waves, maxima in R_{pp} occur at values of τ close to the minima in T_r and T_f (Fig. 11c) and not at an average (or broadband) value of T_d as occurs for the sequential signals (Fig. 11d) that are typical of those in the incoming boundary layer. Thus, although correlations of the boxcar signals have a maximum in R_{pp} at positive τ that corresponds to downstream motion of the shock wave, as well as a second maximum at negative τ corresponding to upstream motion, the shock speeds calculated from these values of τ and ξ are essentially maximum values, not broadband values.

In the Mach 5 cylinder interactions, the maximum upstream and downstream shock speeds deduced from the boxcar correlations are about the same (≈ 100 m/s) and independent of position in the intermittent region. In the Mach 5 facility, 100 m/s is about $0.14U_\infty$. At Mach 3, only cross correlations of the original signals were presented in Ref. 6. Since the shock-induced fluctuations in these signals are also nested, then the negative τ at which the maximum in R_{pp} occurs is also heavily weighted towards the minimum T_r (maximum upstream velocity) rather than the broadband value. Further, it was observed in the Mach 5 study that correlations on the original signal result in a somewhat higher τ (and smaller maximum velocity) than that deduced from correlations of the boxcars. Bearing this in mind, for a spacing of $0.23\delta_o$ (≈ 5.5 mm), a τ of -60 μs in Fig. 10 corresponds to 92 m/s upstream ($\approx 0.16U_\infty$), which correlates well with the Mach 5 result.

In Ref. 7, individual pairs of nested boxcars from the 24-deg compression ramp flow were analyzed and statistics performed on the values of T_r and T_f. The objective was to calculate the probability distribution for the shock speed, but the small number of samples (only 65) precluded an accurate result. The samples obtained gave speeds from $0.05\text{–}0.8U_\infty$ with a mean of about $0.15U_\infty$. Upstream and downstream speeds were about the same. The same calculations have been done on the new Mach 5 data, but in this case the TTM was used to generate the boxcar, and at any station up to 700 pairs of nested boxcars were examined. As in Ref. 7, upstream and

downstream shock speeds were found to be the same, but the average values were lower, about $0.04U_\infty$. This could be due to the small number of samples in Ref. 7 but is more likely due to the use of an STM that biases the results to shorter times and hence higher velocities. Further, at this stage caution is needed in making comparisons since there is no reason to assumer that U_∞ is an appropriate normalizer. Even so, it is clear that in two different flows the shock speeds are essentially the same in both directions and are a small fraction of U_∞.

Andreopoulos and Muck[7] argued that since the shock speeds are of the same order as the velocity fluctuations in the flowfield, this "represents further evidence that the turbulence of the incoming boundary layer is largely responsible for the shock wave motion." However, the shock is an interface and propagates with respect to the fluid at a speed that depends on the upstream and downstream conditions. Hence, this is a questionable conclusion at this stage and is not supported by the results of Tran,[12] who concluded that the shock motion was independent of the large-scale structures of the upstream boundary layer that are convected into the interaction.

IV. Comments on Results

Drawing conclusions from the data set is hampered by the narrow ranges of flow conditions and geometric parameters that any given model type has been tested over. Although no single experiment provides overwhelming evidence of a particular mechanism, the data set as a whole has certain features that warrant future experimental investigation.

Consider first the Mach 3 blunt fin and Mach 5 cylinder results. In a given incoming boundary layer, $(f_c)_{max}$ increases as D decreases. As noted earlier, this suggests a mechanism involving the downstream flowfield and raises the question of how the interaction changes as D increases. Mean wall pressures and surface flow visualization show that the centerline flowfield length scales, the separation location, and the primary vortex scale remain essentially the same in nondimensional form (i.e., normalized by D).[21] Physically, the primary vortex scale increases with D, which might suggest that f_c depends on the length scale of the separated flow. However, results for fixed D but variable δ_o contradict this. In this case, there is little change in the physical length scale, but $(f_c)_{max}$ increases in the thinner boundary layer, and there is a general shift to higher frequencies. Again, this poses the question of how the two flowfields differ, but in this case for fixed D.

The only information on the differences comes from numerical studies.[22] There are no detailed flowfield measurements in blunt-fin interactions. The computations agree well with the complex distributions of $\bar{P}_w$ obtained experimentally, as well as with the separation location and overall length scales, suggesting that the predicted flow structure is probably reliable. The simulations confirm that the scale of the primary vortex does not change as the incoming boundary layer changes, but there are differences in detail. For the thicker boundary layer, there is a larger subsonic region with lower velocities near the upstream edge of the vortex. It is this case that has the lower $(f_c)_{max}$ and the lower range of shock frequencies. Although the computations represent a time-averaged picture, such a result suggests a possible dependence of the shock motion on fluctuations in the "local" properties of the separated flow (i.e., those at the instantaneous upstream boundary) rather than on global properties such as overall length scales. The low shock speeds, and their independence of direction, are also consistent with the idea of turbulent fluctuations in, or global fluctuations of, this embedded subsonic flow region.

The 24-deg compression ramp results seem to be consistent with this idea. First, there is little evidence of any change in shock frequency as the separated bubble increases in length from 2.6 to 4.8 cm. Although the shock dynamics in ramp and blunt-fin flows share common features, the ramp flowfield is structurally quite different. From detailed flowfield surveys in section 2 of the facility (Fig. 11, Ref. 23), the structure of the ramp-induced separation bubble is known, at least in a time-averaged sense. The bubble is very elongated, is effectively embedded in the boundary layer, and has a long, fairly thick region of subsonic flow; extending from S to about $5\delta_o$ downstream of the corner. Close to the wall and near the upstream edge of the bubble, the reversed flow velocities are low with a maximum of about $0.1U_\infty$. The shock center frequency is correspondingly very low, as are the shock speeds. Although flowfield surveys were not made for the ramp further upstream in section 1 of the tunnel, it is probable that the same flow structure is generated since the normalized wall pressures and flow length scales are the same as in section 2. It is also probable that the local conditions near the upstream edge of the bubble are similar in both instances, which would explain why the shock power spectra does not change. However, as α decreases to 20 deg in the same boundary layer, the bubble decreases in scale rapidly (from 2.2 to $0.7\delta_o$) and the shock frequency increases. Although the separation shock wave has the same strength, the subsonic region downstream of it is much smaller.

The higher values of shock frequency seen in the sharp-fin flows using the same boundary layers are also consistent with the above. The sharp-fin flow is characterized by a swept vortical structure. The numerical simulations match the measured surface and flowfield features well and have been used to study the vortical structure.[24] As α increases from 12 to 20 deg, the computed crossflow velocity trajectories show a large increase in the scale of the vortical flow, but as seen in curves 8–10 of Fig. 3, this has no measurable affect on the frequency content of the shock motion. Unlike the separated flow in the 24-deg compression ramp interaction or on centerline in the blunt-fin or cylinder cases, there is no large subsonic region in the sharp-fin case. Both measurements[25,26] and computations[27] show that although the boundary-layer flow downstream of the separation line is highly yawed, it is largely supersonic. If local fluctuations at the upstream boundary of the vortical region play a role, then higher frequencies might be anticipated, since the lower velocity fluid has been swept outboard and this locally supersonic flow is from the outer part of the incoming boundary layer with much higher local mean velocities.

In summary, it must be said that although the dynamics of the shock motion is reasonably well quantified in several different flowfields, the root cause of the unsteadiness is not known for any of them. The low shock zero-crossing frequencies and their variation with model geometry for a fixed boundary layer and the low shock speeds are strongly suggestive of a mechanism involving local or global fluctuations of the turbulent fluid downstream of the separation shock.

New experiments, focused on the investigation of specific mechanisms, are needed to resolve this question. It is unlikely that either simulations or analysis will reveal it, particularly if the mechanism involves fluctuations of, or in, the separated flow region. One such experiment might make use of several pressure transducers aligned streamwise in the intermittent region to monitor shock speed and direction while simultaneously recording fluctuations under the separated shear layer near the instantaneous upstream edge of the separated flow. Through conditional sampling, or other techniques, it could be determined if shock speed and direction correlate with fluctuations in the downstream flow and, more importantly, deduce the order in which these events occur.

Acknowledgments

Support for this work from the Air Force Office of Scientific Research (AFOSR) (Grant 86-0112, monitored by Dr. J. Wilson and Dr. L. Sakell) and from the Center of Excellence in Hypersonics Training and Research (sponsored by NASA, AFOSR, and the Office of Naval Research) are gratefully acknowledged.

References

[1]Bogdonoff, S. M., "Some Experimental Studies of the Separation of Supersonic Turbulent Boundary Layers," Aeronautical Engineering Dept., Princeton Univ., Princeton, NJ, Rept. 336, June 1955.

[2]Chapman, D. R., Kuehn, D. M., and Larson, H. K., "Investigation of Separated Flows in Supersonic and Subsonic Streams with Emphasis on the Effect of Transition," NACA TN-3869, March 1957.

[3]Dolling, D. S. and Orr, C. T., "Unsteadiness of the Shock Wave Structure in Attached and Separated Compression Ramp Flowfields," *Experiments in Fluids,* Vol. 3, No. 4, 1985, pp. 24-32.

[4]Kistler, A. L., "Fluctuating Wall Pressure Under a Separated Supersonic Flow," *Journal of the Acoustical Society of America,* Vol. 36, March 1964, pp. 543-550.

[5]Dolling, D. S. and Murphy, M. T., "Unsteadiness of the Separation Shock Wave Structure in a Supersonic Compression Ramp Flowfield," *AIAA Journal,* Vol. 21, Dec. 1983, pp. 1628-1634.

[6]Muck, K. C., Dussauge, J. P., and Bogdonoff, S. M., "Structure of the Wall Pressure Fluctuations in a Shock-Induced Separated Turbulent Flow," AIAA Paper 85-0179, Jan. 1985.

[7]Andreopoulos, J. and Muck, K. C., "Some New Aspects of the Shock Wave Boundary-Layer Interaction in Compression Ramp Flows," AIAA Paper 86-0342, Jan. 1986.

[8]Dolling, D. S. and Bogdonoff, S. M., "An Experimental Investigation of the Unsteady Behavior of Blunt Fin-Induced Shock Wave Turbulent Boundary-Layer Interactions," AIAA Paper 81-1287, June 1981.

[9]Dolling, D. S. and Narlo, J. C., II, "Driving Mechanism of Unsteady Separation Shock Motion in Hypersonic Interactive Flow," AGARD Conference on Aerodynamics of Hypersonic Lifting Vehicles, AGARD-CP-428, Nov. 1987.

[10]Tran, T. T., Tan, D. K. M., and Bogdonoff, S. M., "Surface Pressure Fluctuations in a Three-Dimensional Shock Wave/Turbulent Boundary-Layer Interaction at Various Shock Strengths," AIAA Paper 85-1562, July 1985.

[11]Tan, D. K. M., Tran, T. T., and Bogdonoff, S. M., "Surface Pressure Fluctuations in a Three-Dimensional Shock Wave/Turbulent Boundary-Layer Interaction," AIAA Paper 85-0125, Jan. 1985.

[12]Tran, T. T., "An Experimental Investigation of Unsteadiness in Swept Shock Wave/Turbulent Boundary Layer Interactions," Ph.D. Dissertation, Mechanical and Aerospace Engineering Dept., Princeton Univ., Princeton, NJ, March 1987.

[13]Chen, C. P., Sajben, M., and Kroutil, J. C., "Shock Wave Oscillations in a Transonic Diffuser Flow," *AIAA Journal,* Vol. 17, Oct. 1979, pp. 1076-1083.

[14]Bogar, T. J., Sajben, M., and Kroutil, J. C., "Characteristic Frequencies of Transonic Diffuser Flow Oscillations," *AIAA Journal,* Vol. 21, Sept. 1983, pp. 1232-1240.

[15]Roos, F. W., "The Buffeting Pressure Field of a High-Aspect-Ratio Swept Wing," AIAA Paper 85-1609, July 1985.

[16]Robertson, J. E., "Characteristics of the Static and Fluctuating-Pressure Environments Induced by Three-Dimensional Protuberances at Transonic Mach Numbers," Wyle Lab., Huntsville, AL, Research Staff Rept. WR-69-3, June 1969.

[17]Speaker, W. V. and Ailman, C. M., "Spectra and Space-Time Correlations of the Fluctuating Pressures at a Wall Beneath a Supersonic Turbulent Boundary Layer Perturbed by Steps and Shock Waves," NASA CR-486, June 1969.

[18]Chyu, W. J. and Hanly, R. D., "Power and Cross Spectra and Space-Time Correlations of Surface Fluctuating Pressures at Mach Numbers Between 1.6 and 2.5," NASA TN-D-5440, Sept. 1969.

[19]Coe, C. F., Chyu, W. J., and Dods, J. B., "Pressure Fluctuations Underlying Attached and Separated Supersonic Turbulent Boundary Layers and Shock Waves," AIAA Paper 73-996, Oct. 1973.

[20]Shewe, G., "On the Structure of Resolution of Wall Pressure Fluctuation Associated with Turbulent Boundary-Layer Flow," *Journal of Fluid Mechanics,* Vol. 134, Sept. 1983, pp. 311-328.

[21]Dolling, D. S. and Bogdonoff, S. M., "Blunt Fin-Induced Shock Wave/Turbulent Boundary-Layer Interaction," *AIAA Journal,* Vol. 20, Dec. 1982, pp. 1674-1680.

[22]Hung, C. M. and Buning, P. G., "Simulation of Blunt Fin-Induced Shock Wave and Turbulent Boundary-Layer Interaction," AIAA Paper 84-0457, Jan. 1984.

[23]Settles, G. S., Vas, I. E., and Bogdonoff, S. M., "Details of a Shock-Separated Turbulent Boundary Layer at a Compression Corner," *AIAA Journal,* Vol. 14, Dec. 1976, pp. 1709-1715.

[24]Horstman, C. C., "Computation of Sharp Fin-Induced Shock Wave/Turbulent Boundary-Layer Interaction," AIAA Paper 86-1032, May 1986.

[25]Oskam, B., "Three-Dimensional Flowfields Generated by the Interaction of a Swept Shock with a Turbulent Boundary Layer," Gas Dynamics Lab. Rept. 1313, Princeton Univ., NJ, Dec. 1976.

[26]Shapey, B. and Bogdonoff, S. M., "Three-Dimensional Shock Wave/Turbulent Boundary-Layer Interaction for a 20-deg Sharp Fin at Mach 3," AIAA Paper 87-0554, Jan. 1987.

[27]Knight, D. D., Horstman, C. C., Shapey, B., and Bogdonoff, S. M., "The Flowfield Structure of the Three-Dimensional Shock Wave Boundary-Layer Interaction Generated by a 20-deg Sharp Fin at Mach 3," AIAA Paper 86-0343, Jan. 1986.